

Growth and morphology of C_{60} crystals

M.A. Verheijen, H. Meekes, G. Meijer, E. Raas and P. Bennema

Research Institute for Materials, Faculty of Science, University of Nijmegen, Toernooiveld, 6525 ED Nijmegen, The Netherlands

Received 31 December 1991

Single crystals of pure C_{60} are grown from the vapour phase. The crystal morphology is compared to the theoretical equilibrium form, predicted on the basis of a periodic bond chain analysis and a statistical mechanical approach. Some interesting growth phenomena are observed and discussed.

1. Introduction

Since Krätschmer et al. [1] discovered a way to synthesize C_{60} and other fullerenes in macroscopic amounts a lot of research has been performed on these new all-carbon molecules [2]. It appeared to be difficult to obtain large crystals of pure C_{60} , however. When the crystals are grown from solution, solvent molecules can be incorporated in the crystal lattice and various crystal structures can result [3–5]. Growth from the vapour phase, on the contrary, can result in pure crystals with a well defined structure [6]. Multiple sublimation steps can be used to assure high purity of the C_{60} material from which the crystals are grown.

At room temperature the C_{60} crystal structure can be regarded as an excellent example of cubic close packing of isotropic spheres because the molecules have almost total rotational freedom in the fcc lattice [7,8]. Moreover, growth from the vapour minimizes the interactions between the crystal interface and the mother phase. For these reasons crystalline C_{60} is well suited to test crystal growth theories. We therefore started to investigate the growth, the morphology and the surface structure of pure C_{60} crystals using optical microscopy and scanning electron microscopy (SEM).

2. Crystal growth

The C_{60} used in this study is obtained via by now

standard procedures [1]. In short, carbon soot is produced in a dc arc discharge between two high purity graphite electrodes in a 0.2 atm He environment. Soxhlet extraction of this soot in boiling toluene is used to separate (mainly) C_{60} and C_{70} from the rest. Liquid column chromatography [9] is used to obtain C_{60} with a purity of at least 99.5%, as checked by mass spectrometry, and NMR and Raman spectroscopy. The C_{60} powder is washed with cyclohexane, to remove any poly aromatic hydrocarbons that might still be present in the sample. About 10 mg of this C_{60} material is placed at the closed end of a 50 cm long, 1 cm diameter quartz tube with four necks at equal distances. The tube is evacuated down to 10^{-5} Torr and heated to 200°C for several hours to remove all the solvent that is embedded in the C_{60} mini-crystallites that are formed after solvent evaporation of the chromatographically separated solution. During all the further heat treatments the quartz tube is kept at low pressure by continuous pumping. The end of the tube that contains the C_{60} powder is placed in a furnace and heated up to 500°C . The vapour pressure of C_{60} is strongly dependent on the temperature [10] and the sublimed C_{60} solidifies in the next section of the quartz tube, which is kept at a $100\text{--}150^{\circ}\text{C}$ lower temperature. Thus a large part of the C_{60} is vapour transported between two sections in an approximately half an hour time period. Surprisingly, about 1/3 of the original material stays behind in the first section even after allowing vapour transport at 500°C for several hours. Although both mass spectrometry and Raman

spectroscopy seem to indicate that the material that stays behind is also C_{60} , we prefer not to use this material any longer as its vapour pressure is somewhat different. We therefore melt off the first segment of the tube, and repeat the vapour transport two more times with the C_{60} material that did vapour transport the first time. Almost all of the latter material can easily be vapour transported into the fourth segment, which is subsequently sealed off on both sides. The isolated very pure C_{60} is then placed in a furnace kept at 500°C for half an hour and cooled down to room temperature in about four hours. Beautiful C_{60} crystals as large as $0.5 \times 0.5 \times 0.5 \text{ mm}^3$ are obtained in this way.

3. The theoretical morphology

The C_{60} crystals have an fcc structure with four molecules per unit cell and cell dimensions of 14.17 \AA (at 300 K) [11]. Starting from this unit cell one can predict the possible crystal faces by means of the periodic bond chain (PBC) theory [12–14]. A PBC is an uninterrupted periodic chain consisting of molecules connected by bonds. Two different intersecting PBCs can form a connected net, i.e. a layer in the crystal lattice with Miller indices (hkl) containing molecules that are all connected with other molecules in this layer. Such a connected net is parallel to a possible crystal face. Considering only nearest neighbour interactions in the crystal lattice two possible types of faces can be expected for an fcc structure, namely $\{111\}$ and $\{200\}$. When next nearest neighbour interactions are taken into account $\{220\}$ forms are also connected and by introducing third nearest neighbour interactions the forms $\{210\}$, $\{311\}$ and $\{531\}$ can also occur. Note that we use the notation $\{200\}$ and $\{220\}$ instead of $\{100\}$ and $\{110\}$ because of the extinction conditions of the space group which will be relevant for the interplanar distances and the roughening temperatures calculated further on.

Using the interaction potential for C_{60} molecules as proposed by Girifalco [15] the bond strengths in the crystal lattice were calculated. For a molecular diameter of 7.04 \AA and a nearest neighbour distance of 10.02 \AA the relative bond strengths of first, second and third nearest neighbour interactions are 1:

$7.8 \times 10^{-2} : 4.4 \times 10^{-3}$. It should be noted that variations within 1% of the values for the molecular diameter and the nearest neighbour distance do not change the relative bond strengths given above. From these numbers it can be concluded that third nearest neighbour interactions can be neglected and second nearest neighbour interactions will only be of minor importance for the morphology.

Given the set of possible faces, one can introduce a further criterion to determine their stability. This is done using a statistical Ising model as proposed by Rijpkema et al. [16,17]. The Ising temperatures of the $\{200\}$, $\{220\}$ and $\{111\}$ faces are calculated, both with and without next nearest neighbour interactions (see table 1). From literature it is known [18–20] that the Ising temperatures are typically about 10% less than the actual roughening temperatures of the faces. As can be seen from table 1 the $\{220\}$ face will be roughened when next nearest neighbour interactions are neglected. If not, an Ising temperature of $6.6 \times 10^2 \text{ K}$ is predicted. This means that at the growth temperature we use (which is approximately 400°C) the $\{220\}$ face will grow roughened or nearly roughened. In both cases the $\{220\}$ face will not occur as a macroscopic face, because its growth velocity will be much larger than the growth velocities of the $\{111\}$ and $\{200\}$ faces as the growth rate of a face increases exponentially just below its roughening temperature [21]. The $\{111\}$ and the $\{200\}$ faces however grow far below their roughening temperatures and are expected to appear on the crystals. By means of a minimalization of the Gibbs free energy the equilibrium form of a crystal can now be obtained. The Gibbs free energy is given by

$$G = N\mu + \sum_{hkl} A_{hkl} \sigma_{hkl},$$

where N is the total number of particles, μ is the

Table 1
Theoretical roughening temperatures for three crystal faces taking into account only nearest neighbour interactions (nn) or both nearest and next nearest neighbour interactions (nnn)

| Face | $T_R(\text{nn})$ (K) | $T_R(\text{nnn})$ (K) |
|-----------|----------------------|-----------------------|
| $\{111\}$ | 2.8×10^3 | 2.8×10^3 |
| $\{200\}$ | 1.9×10^3 | 1.7×10^3 |
| $\{220\}$ | 0.66×10^3 | 0 |

Table 2

Attachment energy and interlayer spacing for the {111} and {200} face

| Face | E_{att} (J) | d_{hkl} (Å) |
|-------|------------------------|---------------|
| {111} | 1.37×10^{-19} | 8.18 |
| {200} | 1.73×10^{-19} | 7.09 |

chemical potential per particle, A_{hkl} is the surface area of a face (hkl) and σ_{hkl} is the specific surface free energy. Minimalization of G means a minimalization of the second term in the equation. The equilibrium crystal form can easily be found now by constructing a Gibbs–Wulff plot, i.e. plotting σ_{hkl} versus orientation. We will take $E_{\text{att}}d_{hkl}$ as a measure for the specific surface free energy σ_{hkl} . Here, d_{hkl} is the distance between two adjacent layers $\{hkl\}$ and E_{att} is the so-called attachment energy or broken bond energy, which is the sum of the energies of the bonds per molecule which lack due to a surface. In table 2 the values of E_{att} and d_{hkl} are given for the {111} and {200} faces. The values for the {220} face are omitted because we want to predict the equilibrium crystal form at the growth temperature which is equal to

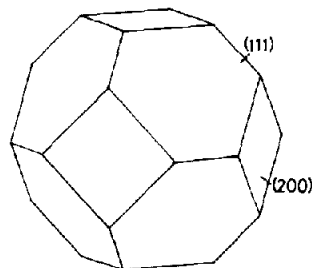


Fig. 1. Theoretical equilibrium crystal form.

or above the roughening temperature of the {220} face. A plot of the thus obtained equilibrium form is given in fig. 1.

4. Experimental morphology and discussion

The crystals have a morphology in accordance with the fcc structure. They have only two different types of faces, namely {111} and {200}. Though the relative sizes of these faces differ strongly between several crystals, the crystal shown in fig. 2 describes the average morphology quite well and it is in good

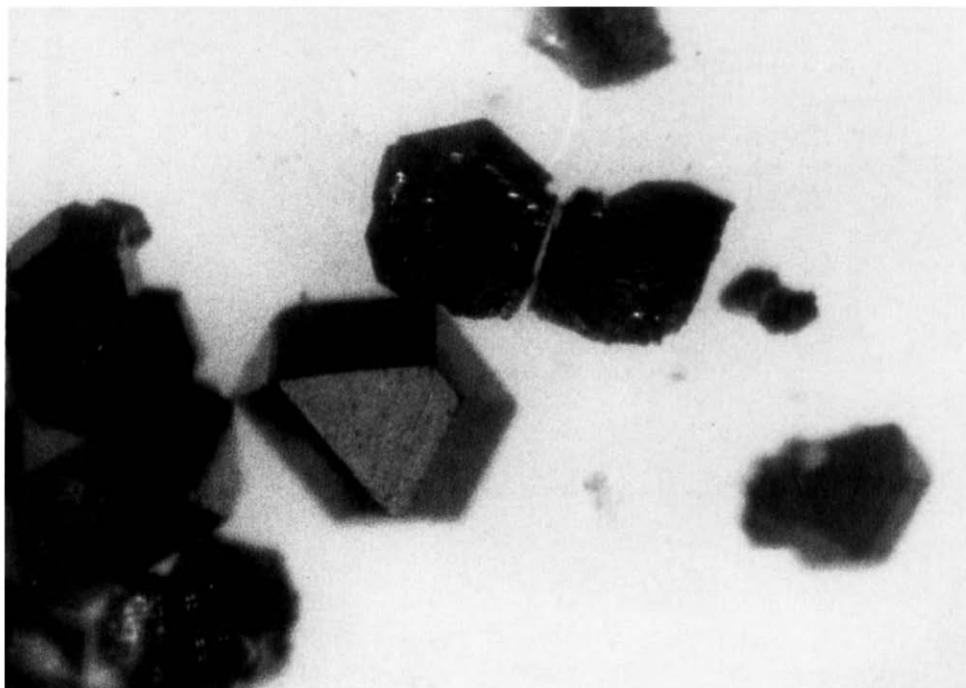


Fig. 2. Average morphology of a C_{60} crystal.

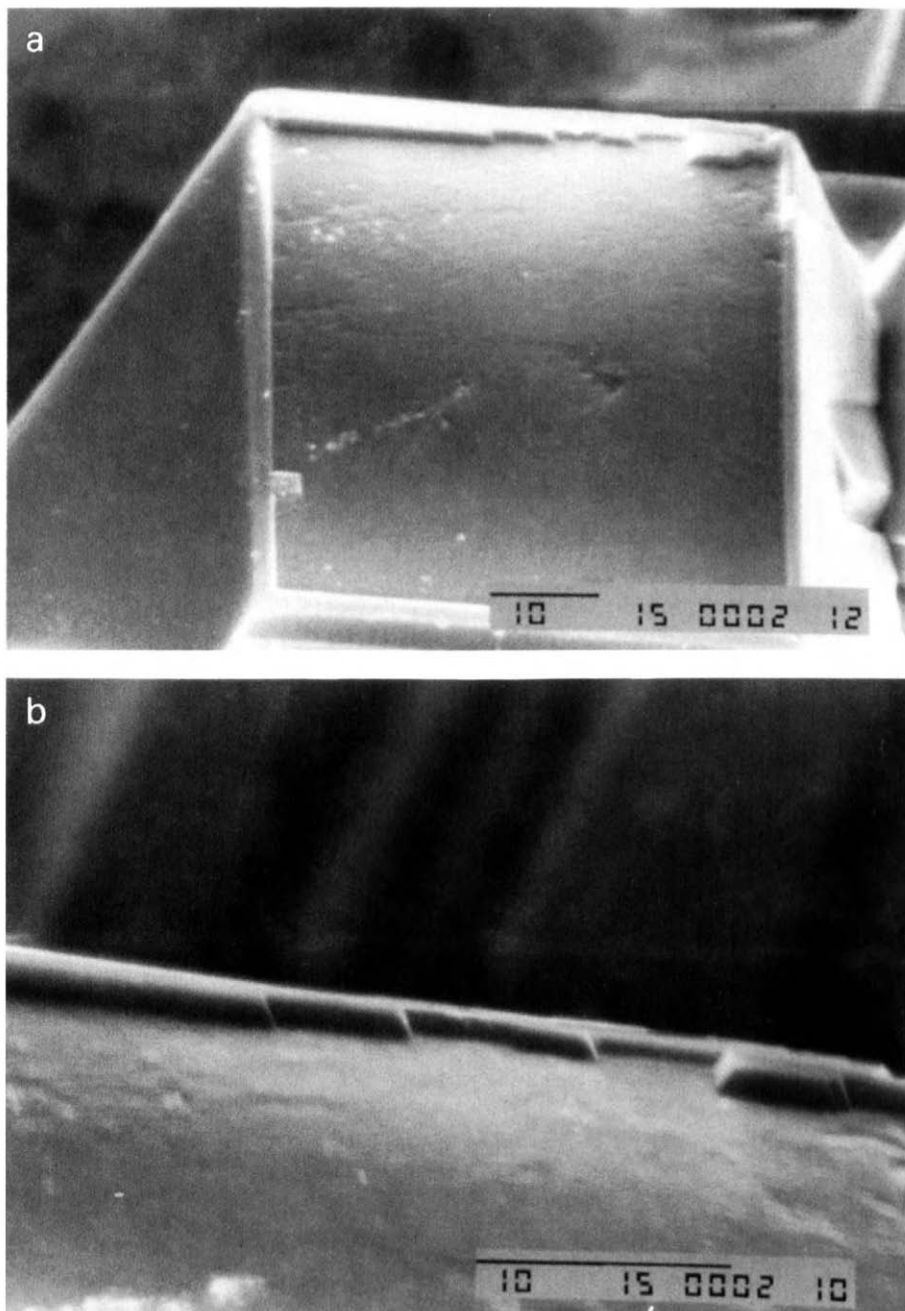


Fig. 3. (a) "Swimming-pool-like" structure on a $\{200\}$ face. (b) Detail of the ridge. In both pictures the black line indicates $10\mu\text{m}$.

agreement with the theoretical equilibrium form of fig. 1 which is surprising because the crystals are grown under circumstances that are far from equilibrium.

SEM studies show that most of the surfaces are very

flat on a microscopic scale when the crystals are grown under the circumstances described above. On some faces macrosteps are seen. Some $\{200\}$ faces have a "swimming-pool-like" shape, i.e. at the edges of the face there is a ridge of about $1\mu\text{m}$ height con-

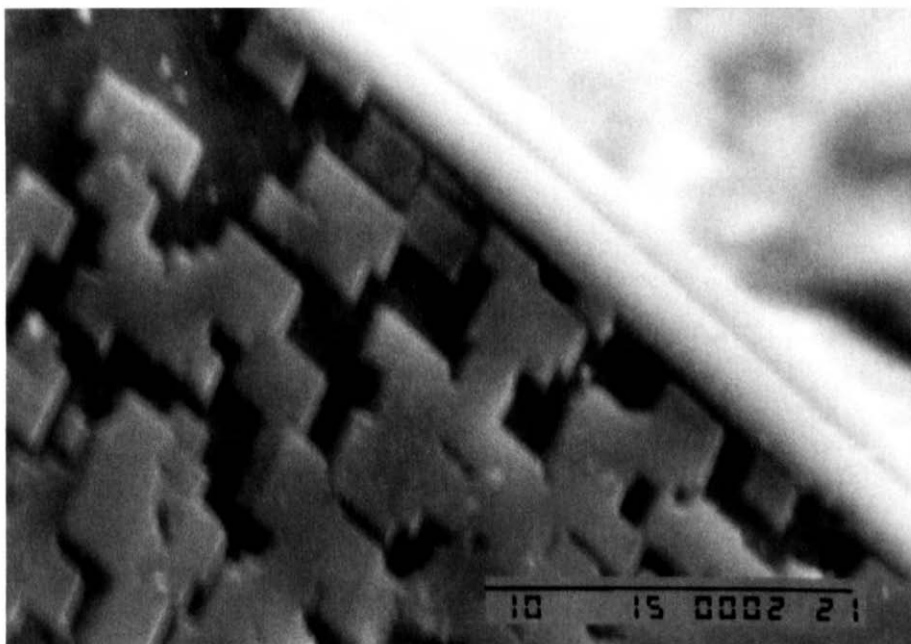


Fig. 4. Growth hillocks on a $\{200\}$ face.

fined by $\{111\}$ and $\{200\}$ faces (see fig. 3). Also rectangularly shaped growth hillocks can be seen on these faces (see fig. 4). These patterns suggest that two dimensional nucleation occurs on $\{200\}$ faces in accordance with a kind of birth and spread model [22,23]. This means that nucleation and spreading of growth layers occur simultaneously. When step bunching takes place at the step edge $\{111\}$ faces can be created. Because the latter are more stable than the $\{200\}$ faces the created side face will grow more slowly than the $\{200\}$ face and thus a growth hillock with $\{111\}$ side faces results. The original bunching of the steps is expected to be due to impurities adsorbed on the $\{200\}$ step edges [24]. The relatively large number of nuclei on the surfaces can either be due to these impurities obstructing the layer growth or by a relatively large driving force which facilitates two-dimensional nucleation.

The appearance of swimming-pool-like shapes on the $\{200\}$ surfaces can be explained by a relatively low temperature at the edges in comparison with the middle of a crystal face and therefore a higher local driving force for crystallization. This temperature difference is due to a larger surface area per unit volume at the edges resulting in a more effective radia-

tive cooling, this effect being stronger the faster the crystal is growing. It is also possible that at the corners due to steep gradients in the vapour concentration, a higher transport of growth units occurs than at the centre. At the corners two-dimensional nucleation may occur. In both cases the $\{111\}$ faces are the most stable, resulting in ridges on the $\{200\}$ faces.

A further observation is the frequent appearance of twinned crystals. This twinning occurs mostly in the form of two individuals. The twinning plane connecting the two parts is a common $\{111\}$ plane. The twinning is observed as one individual being rotated over 60° around the $[111]$ axis with respect to the other individual. This sixfold rotation can be explained by a stacking fault, for which in one single plane the cubic close packing is disturbed by the hexagonal one.

Acknowledgement

We gratefully acknowledge the financial support of the Netherlands Organization for Scientific Research (NWO/SON) and the Dutch Foundation for Fundamental Research of Matter (FOM).

Note added

Recently a similar procedure to grow large, pure C_{60} crystals has been described by Meng et al. [25].

References

- [1] W. Krätschmer, L.D. Lamb, K. Fostiropoulos and D.R. Huffman, *Nature* 347 (1990) 354.
- [2] R.E. Smalley, The almost (but never quite) complete buckminsterfullerene bibliography, available upon request ("Buckybib", Department of Chemistry, Rice University, P.O. Box 1892, Houston, TX 77251, USA).
- [3] R.M. Fleming, A.R. Kortan, B. Hessen, T. Siegrist, F.A. Thiel, P. Marsh, R.C. Haddon, R. Tycko, G. Dabbagh, M.L. Kaplan and A.M. Mujsce, *Phys. Rev. B* 44 (1991) 888.
- [4] J.M. Hawkins, T.A. Lewis, S.D. Loren, A. Meyer, J.R. Heath, R.J. Saykally and F.J. Hollander, *J. Chem. Soc. Chem. Commun.* (1991) 775.
- [5] S.M. Gorun, K.M. Creegan, R.D. Sherwood, D.M. Cox, V.W. Day, C.S. Day, R.M. Upton and C.E. Briant, *J. Chem. Soc. Chem. Commun.* (1991) 1556.
- [6] R.M. Fleming, T. Siegrist, P.M. Marsh, B. Hessen, A.R. Kortan, D.W. Murphy, R.C. Haddon, R. Tycko, G. Dabbagh, A.M. Mujsce, M.L. Kaplan and S.M. Zahurak, *Mater. Res. Soc. Symp. Proc.* 206 (1991) 691.
- [7] C.S. Yannoni, R.D. Johnson, G. Meijer, D.G. Bethune and J.R. Salem, *J. Phys. Chem.* 95 (1991) 9.
- [8] R. Tycko, R.C. Haddon, G. Dabbagh, S.H. Glarum, D.C. Douglass and A.M. Mujsce, *J. Phys. Chem.* 95 (1991) 518.
- [9] H. Aije, M.M. Alvarez, S.J. Anz, R.K. Beck, F. Diederich, K. Fostiropoulos, D.R. Huffman, W. Krätschmer, Y. Rubin, K.E. Schriver, D. Sensharma and R.L. Whetten, *J. Phys. Chem.* 94 (1990) 8630.
- [10] C. Pan, M.P. Sampson, Y. Chai, R.H. Hauge and J.L. Margrave, *J. Phys. Chem.* 95 (1991) 2944.
- [11] P.A. Heiney, J.E. Fischer, A.R. McGhie, W.J. Romanov, A.M. Denenstein, J.P. McCauley Jr., A.B. Smith III and D.E. Cox, *Phys. Rev. Letters* 66 (1991) 2911.
- [12] P. Hartman and W.G. Perdok, *Acta Cryst.* 8 (1955) 49, 521, 525.
- [13] P. Hartman, *Z. Krist.* 119 (1963) 65.
- [14] P. Hartman, in: *Crystal growth: an introduction*, ed. P. Hartman (North-Holland, Amsterdam, 1973) p. 367.
- [15] L.A. Girifalco, *J. Phys. Chem.* 95 (1991) 5370.
- [16] J.J.M. Rijpkema, H.J.F. Knops, P. Bennema and J.P. van der Eerden, *J. Cryst. Growth* 61 (1982) 295.
- [17] P. Bennema, in: *Sir Charles Frank, an eightieth birthday tribute*, eds. R.G. Chambers, J.E. Enderby, A. Keller, A.R. Lang and J.W. Steeds (Hilger, Bristol, 1991) p. 46.
- [18] J.D. Weeks and G.H. Gilmer, in: *Advances in chemical physics*, eds. I Prigogine and S.A. Rice (Wiley, New York, 1979) p. 157.
- [19] H. van Beijeren, *Commun. Math. Phys.* 40 (1975) 1.
- [20] J.P. van der Eerden, P. Bennema and T.A. Cherapanova, *Progr. Cryst. Growth Charact.* 1 (1978) 219.
- [21] P. Bennema and J.P. van der Eerden, in: *Morphology of crystals*, ed. I. Sunagawa (Terrapub, Tokyo, 1987) ch. 1.
- [22] G.H. Gilmer and P. Bennema, *J. Appl. Phys.* 43 (1972) 1347.
- [23] S.W.H. de Haan, V.J.A. Meeuwse, B.P.Th. Veltman, P. Bennema, C. van Leeuwen and G.H. Gilmer, *J. Cryst. Growth* 24 (1974) 491.
- [24] J.P. van der Eerden and H. Müller-Krumbhaar, in: *Morphology and growth unit of crystals*, ed. I. Sunagawa (Terrapub/Reidel, Tokyo/Dordrecht, 1989) p. 133.
- [25] R.L. Meng, D. Ramirez, X. Jiang, P.C. Chow, C. Diaz, K. Matsuishi, S.C. Moss, P.H. Hor and C.W. Chu, *Appl. Phys. Letters* 59 (1991) 3402.